# Relating high ozone, ultrafine particles, and new particle formation episodes using cluster analysis

Cristina Carnerero [a,b,*], Noemí Pérez [a], Tuukka Petäjä [c], Tiia M. Laurila [c], Lauri R. Ahonen [c], Jenni Kontkanen [c], Kang-Ho Ahn [d], Andrés Alastuey [a], Xavier Querol [a]

[a] Institute of Environmental Assessment and Water Research (IDAEA-CSIC), Barcelona, 08034, Spain
[b] Department of Civil and Environmental Engineering, Universitat Politècnica de Catalunya, Barcelona, 08034, Spain
[c] Institute for Atmospheric and Earth System Research (INAR) / Physics, Faculty of Science, University of Helsinki, 00014, Finland
[d] Department of Mechanical Engineering, Hanyang University, Seoul, Republic of Korea

ABSTRACT

We studied the simultaneity of tropospheric ozone ($O_3$) episodes, high ultrafine particle (UFP; diameter < 100 nm) concentrations, and the occurrence of new particle formation at a regional background station in the Western Mediterranean (northeast Spain), which is affected considerably by the transport of pollutants emitted in the Barcelona metropolitan area and nearby populated and industrial areas. Using cluster analysis, we categorized summer and spring days between 2014 and 2018 according to their daily cycles of $O_3$ concentrations, and then studied the evolution of the particle number size distribution, meteorological variables, and black carbon and sulfur dioxide concentrations. The analysis revealed that, in spring and summer, the highest UFP concentrations coincided with the highest $O_3$ episodes, but new particle formation was largely inhibited during these episodes, probably due to the high aerosol pollution load transported from the Barcelona metropolitan area to the station. In contrast, new particle formation episodes were concurrent with the lowest concentrations of $O_3$ and UFPs, including the number of particles in the 9–25 nm size range. Measurements carried out in an intensive field study, using an air ion spectrometer and a particle size magnifier, support these results. In addition, measurements obtained onboard tethered balloons revealed that sea and land breezes transported regional pollutants vertically up to about 400 m above ground level. This coincided with episodes of vertical recirculation of air masses that lasted for several days, which resulted in high $O_3$ and high UFP episodes, while new particle formation was inhibited.

## 1. Introduction

Ultrafine particles (UFPs; particles less than 100 nm in diameter) are not included in air quality regulations, but they have considerable potential for affecting health (Atkinson et al., 2010; Lanzinger et al., 2016; Stafoggia et al., 2017; Tobías et al., 2018). In urban areas, the main source of primary UFPs is road traffic (Pey et al., 2009; Dall'Osto et al., 2012; Kumar et al., 2014; Salma et al., 2014; Ma and Birmili, 2015; Paasonen et al., 2016). Industrial emissions (Keuken et al., 2015b), airports (Keuken et al., 2015a), harbors (Kecorius et al., 2016), and biomass burning (Pöschl, 2005) also contribute significantly to the increase in UFP concentrations. Furthermore, photochemical formation of new particles may also exert a large influence on ambient levels of UFPs in urban and regional environments (Dall'Osto et al., 2013; Salma et al.,

2016; Kerminen et al., 2018; Chu et al., 2019), and even dominate the total particle number concentrations at a global scale (Gordon et al., 2017). Here, we use the term UFP episodes to designate the periods when number concentration (not necessarily particulate matter mass) markedly increases over the (usually low) regional background particle number concentration (2000–3000 $cm^{-3}$). These episodes may be caused by new particle formation bursts or by regional transport of air masses and plumes polluted with UFP particles.

Tropospheric ozone ($O_3$) is a secondary pollutant originating from the chemical reaction of precursors, such as volatile organic compounds (VOCs), carbon monoxide (CO), and nitrogen dioxide ($NO_2$). It is estimated that 95–98% of the population is exposed to $O_3$ levels exceeding the World Health Organization (WHO) guidelines for the protection of human health (100 $\mu g\,m^{-3}$ as an 8-h moving average; WHO, 2006),

while according to the European Union (EU) target value (120 µg m$^{-3}$ as an 8-h moving average; human health target value), 7–30% of the population is exposed EEA, 2018). The EU specifies two additional target values for tropospheric O$_3$: a public information threshold of 180 µg m$^{-3}$ h$^{-1}$ and an alert threshold of 240 µg m$^{-3}$ h$^{-1}$.

Given their largely secondary origin, characterization of O$_3$ and photochemical UFP pollution episodes is highly complex, creating challenges for defining effective strategies to abate the ambient concentrations of the pollutants. The Western Mediterranean is particularly exposed to photochemical O$_3$ and UFP episodes due to its climate of high insolation and low precipitation. Furthermore, its complex topography, with steep valleys oriented in the same direction as the diurnal sea breeze, allows pollution emitted in the densely populated coastal areas to be channeled inland, especially in the summer (Millán et al., 1991). In addition to urban and industrial emissions, high levels of nitrogen oxide (NOx) and sulfur dioxide (SO$_2$) emissions are associated with shipping in the Mediterranean. The area is also characterized by relatively high biogenic VOC emissions in the summer, compared to other Mediterranean forests and mixed forests in Europe and the US (Seco et al., 2011). Therefore, the atmospheric and geographic patterns of this area create conditions that allow for the production of high O$_3$ concentrations and UFP regional episodes, the latter due to new particle formation (NPF) and/or transported UFP-polluted air masses.

Previous studies on particle number size distribution (PNSD) time series in high insolation urban areas revealed the frequent simultaneous occurrence of photochemical NPF and O$_3$ episodes in the spring and summer (Minoura and Takekawa, 2005; Park et al., 2008; Pey et al., 2009; Fernández-Camacho et al., 2010; Wonaschütz et al., 2015; Wang et al., 2016). In a cluster analysis, Brines et al. (2015) reported that average O$_3$ concentrations reached their highest levels in the NPF cluster in most of the cities studied during periods of high solar insolation, temperatures, and wind speeds, and when humidity was low and the concentrations of other pollutants (e.g., CO, NOx, particulate matter mass, and black carbon [BC]) were at background levels. It should be noted that these studies usually covered the whole year, and, therefore, the simultaneous seasonal peaking of O$_3$ and UFPs may be due to either similarities in seasonal patterns of these photochemically driven pollutants or the same atmospheric processes causing both pollution episodes. However, O$_3$ formation peaks under the presence of high concentrations of precursors (Monks et al., 2015), whereas NPF depends on the balance between the rates of formation of clusters and the rates of loss to pre-existing surfaces. In areas with low precursor concentrations, thus low formation rates, NPF requires clean atmospheres, so that loss rates do not outweigh formation rates (Boy and Kulmala, 2002).

Carnerero et al. (2018) and Querol et al. (2018) studied NPF and O$_3$ in Madrid in July 2016, and found that even though O$_3$ concentrations were high throughout the period, NPF only occurred with relatively low O$_3$ episodes. According to this analysis, NPF and O$_3$ peaks were out of phase, i.e., relative minimum concentrations of O$_3$ coincided with periods with NPF, and relative maximum concentrations of O$_3$ corresponded to periods without NPF. To understand the interconnections at a deeper level, in this study we focus on the warm seasons in the period 2014–2018 to investigate the relationship between episodes of O$_3$, UFPs, and NPF in the northern region of the Barcelona Province (northeast Spain), where these episodes occurred with a relatively high frequency. In the last decade, the O$_3$ threshold for health protection of the European Air Quality Directive (120 µg m$^{-3}$ for the maximum 8 h moving daily averages in less than 25 days as an average for 3 years) was consistently exceeded in the study area. In 2015–2018, 34 to 40 days of exceedance per year, mostly concentrated in June and July, were recorded in the monitoring site of this study. Data on episode frequency for UFP and NPF are not available for the regional background. For the nearest urban background, the frequency of NPF bursts has been estimated to reach 15% of the time on an annual basis, mainly in spring and summer (Brines et al., 2015).

As stated above, previous studies have found a clear relationship between NPF episodes and high O$_3$ levels. Given that these studies covered annual periods, the O$_3$–NPF correlation may be due merely to the fact that both are maximized in spring and summer or that the occurrence of episodes of high O$_3$ and NPF are interrelated. O$_3$ levels may, directly or indirectly, play a key role in NPF by increasing OH radicals; however, our focus here is to determine the relationships between the most intense O$_3$ and NPF episodes, rather than all episodes. Thus, the main objectives of this study are to identify the highest episodes of NPF, UFP, and O$_3$ using long time series of O$_3$ and size-segregated UFP obtained during the warm season, and to investigate commonalities and differences in the patterns of these events. Furthermore, we use data from a field study that provide information on vertical profiles of O$_3$ and UFP during 10–14 July 2017 to support the interpretations of the relationship between UFP and O$_3$ in these photochemical pollution episodes.

## 2. Methodology

### 2.1. The study area

The data presented in this study were obtained at Montseny (MSY; 41°46′45.63″N, 02°21′28.92″E, 720 m a.s.l.), a regional background monitoring station established in 2002. The station is included in the European Aerosols, Clouds and Trace gases Research InfraStructure network (ACTRIS), the Global Atmosphere Watch network (GAW), and the atmospheric pollution monitoring and forecasting network of the Government of Catalonia (XVPCA). Montseny is considered a good representation of regional environments in the Western Mediterranean Basin (Pérez et al., 2008).

Montseny is located in a rural environment in a valley oriented in a northwest–southeast direction. It lies in the Montseny Natural Park, 40 km northeast of Barcelona and 30 km northwest of the Mediterranean coastline. The site is densely forested, the prominent vegetation being holm oak (*Quercus ilex* L.). The area around Montseny is restricted to traffic; the closest road is located 3 km from the station. The main sources of pollutants from the nearby Barcelona metropolitan area (BMA) are road traffic and industries, with additional contributions from aircraft, shipping, biomass burning, power generation, and livestock.

In the absence of strong synoptic winds, sea and mountain breezes are the main factors that determine the atmospheric dynamics at Montseny, which in turn regulate the daily evolution of pollutant concentrations. For this reason, the station is frequently affected by anthropogenic emissions originating from the valley and the BMA, channeled northward due to the complex orography. Previous studies have demonstrated that, without dominant synoptic winds, the sea breeze may transport polluted air masses up to the Pyrenees (>3000 m) and inject them at high altitudes, from where they are transported by mesoscale winds toward the Mediterranean Sea and sink due to subsidence. The following day, the sea and land breezes can transport the aged polluted air mass inland, closing the recirculation and causing high O$_3$ (Millán et al., 1997, 2000; Toll and Baldasano, 2000; Gonçalves et al., 2009; Valverde et al., 2016; Querol et al., 2017) and particulate matter episodes (Rodríguez et al., 2003) in the Western Mediterranean. This phenomenon is most favored in the spring and summer, when synoptic winds are frequently absent in the area, and the sea and land breezes are stronger as a consequence of maximal solar radiation. Hemispheric transport and stratospheric intrusions also contribute, to a lesser extent, to O$_3$ concentrations (Kalabokas et al., 2007, 2017; Querol et al., 2017, 2018).

### 2.2. Instrumentation

From April to September 2014–2018, part of the permanent instrumentation at Montseny was used. Particle number size distribution in the size range 9–856 nm (N) was measured continuously every 5 min

**Table 1**
Occurrences of new particle formation (NPF) events in absolute numbers and percentages according to ozone ($O_3$) clusters (see Table 2 for characteristics of the clusters). The sum of values for the categories for each cluster may not total 100% due to rounding. The total number of days in each cluster is also shown.

| NPF category | Extreme $O_3$ | High $O_3$ | Mild $O_3$ | Low $O_3$ |
|---|---|---|---|---|
| No data | 7 (11.9%) | 31 (14.2%) | 57 (16.2%) | 51 (21.8%) |
| Nonevent | 43 (72.9%) | 144 (66.1%) | 214 (60.8%) | 132 (56.4%) |
| Undefined | 2 (3.4%) | 6 (2.8%) | 10 (2.8%) | 3 (1.3%) |
| Burst | 6 (10.2%) | 22 (10.1%) | 31 (8.8%) | 20 (8.5%) |
| Class II | 1 (1.7%) | 7 (3.2%) | 10 (2.8%) | 8 (3.4%) |
| Class I | 0 (0.0%) | 8 (3.7%) | 30 (8.5%) | 20 (8.6%) |
| Total number of days | 59 | 218 | 352 | 234 |

with a scanning mobility particle spectrometer (SMPS; TROPOS) connected to a condensation particle counter (CPC; TSI 3772). $O_3$ was measured with a photometry-based analyzer (MCV 48AV); $SO_2$ was measured with a UV fluorescence analyzer (Teledyne T100); BC was determined with a multi-angle absorption photometer (MAAP; Thermo Scientific). All the inlets were located at 3.5 m above ground level. The station was also equipped with an automatic meteorological station placed at 10 m above ground level (Vantage Pro Plus; Davis Instruments).

In addition, an intensive field study was carried out from 12 June to 31 July 2017 at a location 250 m east of the station. During the study, an air ion spectrometer (AIS; AIREL Ltd; Mirme et al., 2007) measured the mobility distribution of ambient ions in the size range 0.8–40 nm. A particle size magnifier (PSM; Airmodus Ltd., Vanhanen et al., 2011) was used to measure the number size distributions of charged and neutral particles in the size range 1.15–2.6 nm and total number concentration above 1.15 nm. The PSM was installed together with an inlet system, comparable to one described in Kangasluoma et al. (2016), incorporating an automatic zero measurement and a core sampling (an inlet system with a bypass flow, on/off ion filter, and a flow system to automate background measurement) to minimize sampling losses. Prior to the field study, the PSM was calibrated with tungsten oxide particles produced with a hot wire generator (e.g., Kangasluoma et al., 2015).

In addition, from 10 to 14 July, the vertical distribution of pollutants up to 2 km was measured using miniaturized instrumentation suspended from two tethered balloons. A miniaturized butanol-based CPC (Hy-CPC; Hanyang University; Lee et al., 2014) measured the number concentration of particles with diameters > 3 nm ($N_3$). The measurements had a time resolution of 1 s and a sample flow of 0.125 L min$^{-1}$. $O_3$

concentrations were measured with a photometry-based personal ozone monitor (POM; 2B Technologies). The balloons were also equipped with a global positioning system (GPS), a thermometer, hygrometer, barometer, anemometer, and wind vane. Each profile took approximately 15 min from the surface to the maximum altitude. When there were high horizontal winds during the sounding, the balloons were dragged horizontally instead of ascending, and the sounding time increased.

### 2.3. Data analysis

For the cluster analysis, we considered the period 2014–2018. We only used data between April and September to focus on periods of high photochemical activity and high insolation, and, therefore, high concentrations of the pollutants of interest. All times are expressed in local time (UTC + 2 h), unless otherwise stated.

K-means clustering was applied to the daily $O_3$ hourly concentration averages. The K-means algorithm divides a set of $n$ samples into $K$ clusters $C = \{C_1, C_2, ..., C_K\}$ of equal variance, minimizing the sum of squared distances of the samples to their closest cluster center, described by the mean of the samples $\mu_j$:

$$\sum_{i=0}^{n} \min_{\mu_j \in C} |x_i - \mu_j|^2$$

We used the Python module *Scikit-learn* (Pedregosa et al., 2011) to implement the K-means algorithm. The number of clusters $K$ has to be decided by the user. $K$ was chosen so that only one cluster contained all the days registering an exceedance of the "information value" (180 µg m$^{-3}$ h$^{-1}$) fixed by the EU 2008/50/CE Directive, using the minimum number of clusters. This was achieved by using $K = 10$ clusters. Despite being statistically different, some of these initial 10 clusters represented similar atmospheric conditions. For this reason, we reduced the number of clusters by grouping similar clusters, i.e., clusters that shared similar patterns in all or most of the variables considered. To that end, for each set of days corresponding to the same cluster, we studied the average values of all the other variables available in order to characterize every cluster (Fig. S1 and Table S1). With this information, we were able to detect similar clusters and group them. Note that the original cluster containing all the $O_3$ information value exceedances was not grouped with any other cluster. More information on the original clusters and grouping can be found in the supplementary material. Eventually, four different situations leading to distinct $O_3$ daily patterns were identified with four cluster groups: days with an exceedance of the information value ("extreme" cluster), days with high $O_3$ levels without

**Table 2**
Qualitative summary of the days in each ozone ($O_3$) cluster (see also Fig. 1).

| | Extreme $O_3$ | High $O_3$ | Mild $O_3$ | Low $O_3$ |
|---|---|---|---|---|
| Number of days | 59 | 218 | 352 | 234 |
| Temporal distribution | June and July | Mainly in summer | Mainly in spring and autumn | Spring and autumn |
| Days with exceedances of the EU information value[a] | 8 | 0 | 0 | 0 |
| Days with exceedances of the EU target value[b] | 59 | 104 | 12 | 0 |
| Temperature | Highest | Intermediate | Intermediate | Lowest |
| Relative Humidity | Lowest | Low | High | Highest |
| Wind speed | Highest | High | Intermediate | Lowest |
| Solar radiation | Highest | High | High | Lowest |
| $N_{9-855}$ | Highest | Intermediate | Intermediate | Lowest |
| $N_{9-25}$ | Highest | High | Intermediate | Lowest |
| CS | Highest | Intermediate | Intermediate | Lowest |
| BC | Highest | Intermediate | Intermediate | Lowest |
| $SO_2$ | Highest | Intermediate | Low | Low |
| Comments | Very hot and dry summer days, strong breezes cause transport of pollutants | Warm and dry days, breezes cause transport of pollutants | Mild temperature and humidity, light breezes may transport pollutants | Cool and humid days with no transport of pollutants |

[a] European Union (EU) information value: hourly $O_3$ concentration average exceeds 180 µg m$^{-3}$.

[b] EU target value: $O_3$ concentrations exceed 120 µg m$^{-3}$ for the maximum 8 h moving daily averages in at least 25 days as an average for 3 years.
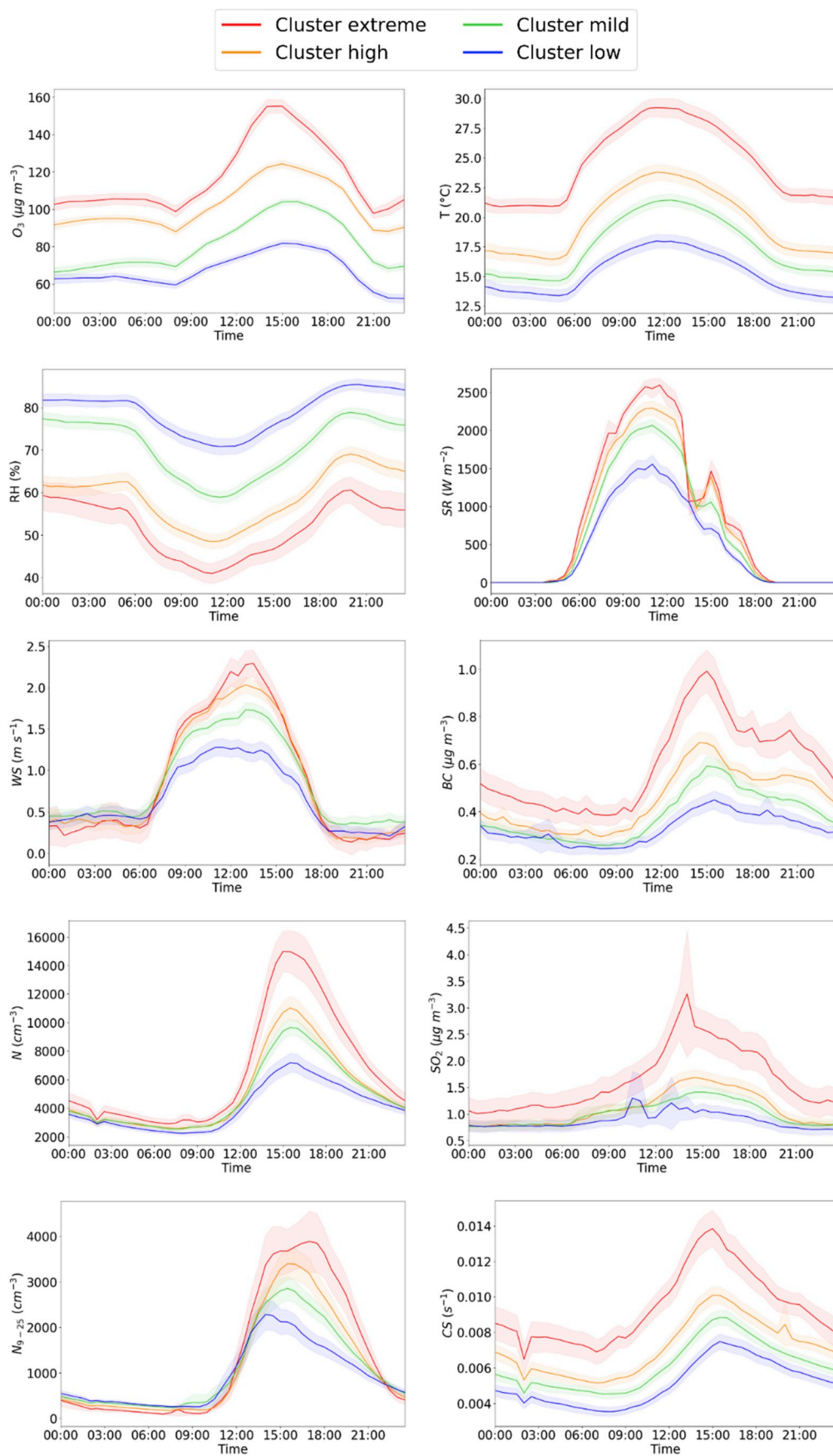
**Fig. 1.** Average daily evolutions of ozone ($O_3$), temperature (T), relative humidity (RH), solar radiation (SR), wind speed (WS), black carbon (BC), particle number concentration (N), sulfur dioxide ($SO_2$), particle number concentration of the nucleation mode ($N_{9-25}$), and the condensation sink (CS) at Montseny between April and September 2014–2018. Data are shown separately for the clusters determined from K-means cluster analysis (cluster characteristics are shown in Table 2). Shaded areas represent 95% confidence intervals.
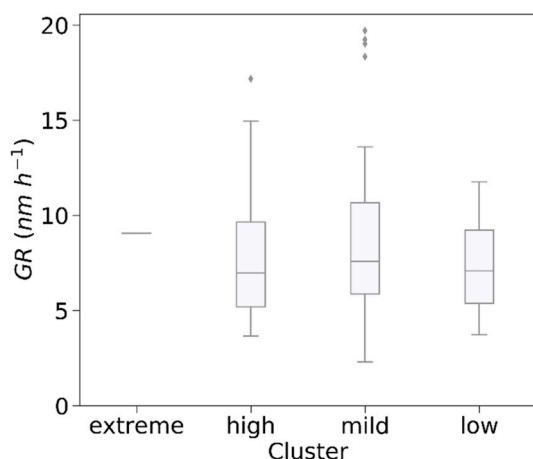
**Fig. 2.** Boxplot of particle growth rates (GRs) of Class I and Class II new particle formation (NPF) events according to their corresponding cluster classification for the period between April and September 2014–2018. The boxes show the three quartiles of the distribution, while the whiskers extend to 1.5 times the interquartile ranges. Values outside this range are shown as outliers. For the "extreme" cluster, only one value is shown because only one NPF episode was identified. Cluster characteristics are given in Table 2.

exceedances ("high" cluster), days with moderate $O_3$ concentrations ("mild" cluster), and days with low $O_3$ levels ("low" cluster).

Using the PNSD, we calculated the total number concentration of particles in the size range 9–855 nm (N), the number concentration of UFP ($N_{9-100}$), the nucleation-mode concentration, here considered as the concentration of particles in the size range 9–25 nm ($N_{9-25}$), and the condensation sink (CS, the frequency with which condensable vapor molecules condense on existing particles; Kulmala et al., 2012).

NPF episodes were manually classified according to a scheme adapted from that of Dal Maso et al. (2005). Days with clear particle formation and growth were classified as Class I. If the mode, concentration, or diameter fluctuated strongly during NPF, the day was classified as Class II. Days without a nucleation mode (<25 nm) lasting for at

least 1 h were classified as nonevent. Days with a nucleation mode that did not grow with time were classified as undefined. In addition to this classification, we considered an extra NPF category for burst-like events. Burst events are similar to short Class I events lasting for about 1 h, in which there is clear NPF that stops rapidly (see example in Fig. S2). This may be due to either a change of air mass after particles have formed locally (the air mass is coming from a region where NPF has not occurred, and the newly formed particles are transported elsewhere) or the sudden dilution of the particles after sunrise. These bursts were not registered with increases in BC, and, therefore, cannot be associated with local emissions such as those from nearby vehicles. Burst events would be considered nonevents according to the scheme proposed by Dal Maso et al. (2005) if they lasted for less than 1 h. However, we regarded them as a separate category because they were observed about three times per month on average during the period of study. Finally, days that could not be clearly categorized were classified as undefined.

Log-normal modes were fit to the daily PNSD using the algorithm proposed by Hussein et al. (2005). The modes were used to calculate growth rates (GR) for all Class I and Class II NPF events.

## 3. Results

### 3.1. Data clustering

In classifying NPF events, a total of 717 daily PNSDs were classified, out of which 533 were categorized as non-NPF events (74% of the days for which data were available). Only 84 days (12%) were classified as Class I or Class II events, and 79 days were classified as burst events (11%). The rest (3%) were classified as undefined NPF events. The number of days in each NPF event category and the percentages according to each cluster are shown in Table 1. These results are in agreement with those reported in other European studies (see e.g., Manninen et al., 2010; Németh et al., 2018; Nieminen et al., 2018; Pikridas et al., 2012; Wonaschütz et al., 2015), with NPF ranging from 10 to 57% of the days for which data were available. However, a direct comparison with these studies is not possible, because most give annual or seasonal data, whereas in this study we considered data for only
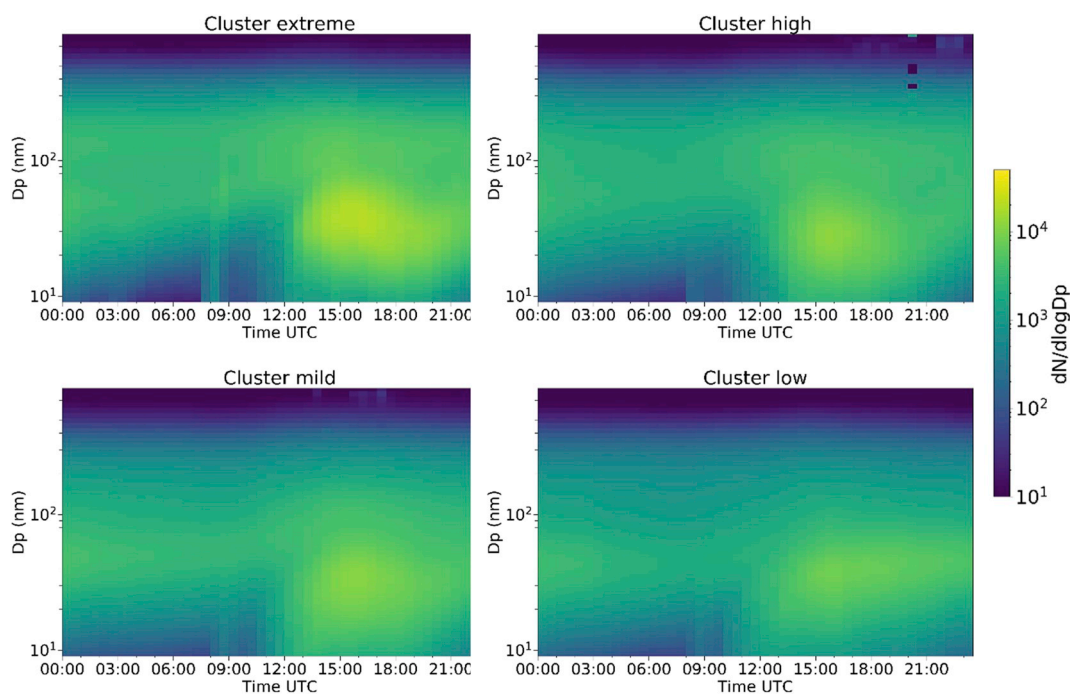


**Fig. 3.** Average particle number size distribution for the days in each cluster at Montseny between April and September 2014–2018. Cluster characteristics are given in Table 2.
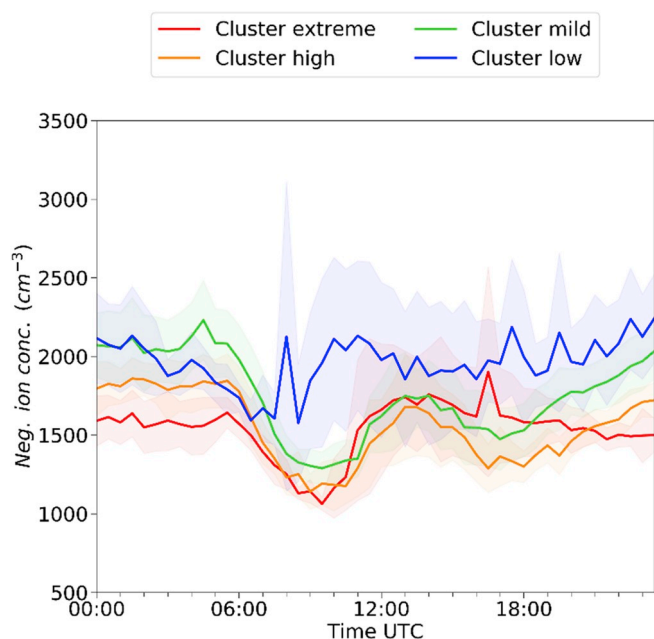
**Fig. 4.** Average daily cycles of the concentration of negative ions in the size range 0.8–40 nm, measured with an air ion spectrometer and shown by cluster classification, during an intensive field study from 12 June to 31 July 2017. Shaded areas represent 95% confidence intervals. Cluster characteristics are given in Table 2.
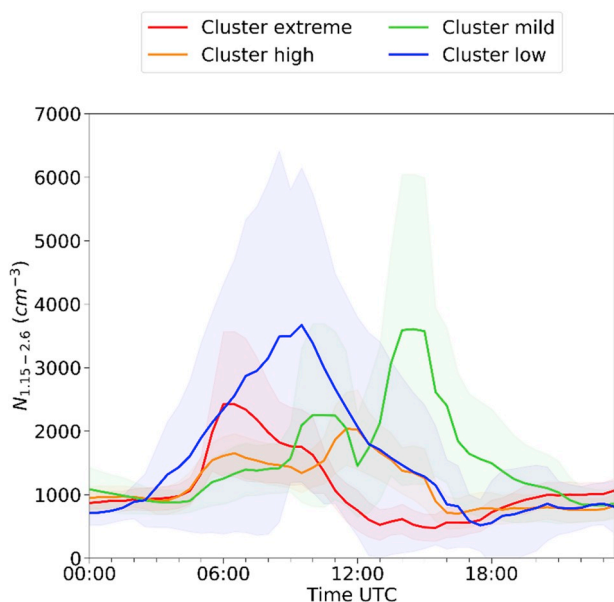


**Fig. 5.** Average daily cycles of particle number concentration in the size range 1.15–2.6 nm (N1.15-2.6), measured with a particle size magnifier shown by cluster classification, during an intensive field study from 12 June to 31 July 2017. Shaded areas represent 95% confidence intervals. Cluster characteristics are given in Table 2.

April–September. Moreover, we considered burst events as a separate category, which would have been classified as events or non-events in other studies (see Table 1).

The results of the $O_3$ cluster analysis are presented in Fig. 1, showing the average daily cycles of $O_3$, temperature, relative humidity, wind speed, solar radiation, BC, $SO_2$, CS, N, and $N_{9-25}$. A qualitative summary of the results shown in this figure can be found in Table 2. Fig. 2 shows the particle growth rates for the days that registered Class I or Class II

NPF, according to their corresponding cluster. Fig. 3 represents the average 30 min PNSD calculated for each cluster separately.

The $O_3$ daily pattern in the "extreme" cluster was found only in June and July in a total of 59 days (7% of the period). This is the only cluster registering $O_3$ exceedances of the hourly information threshold (180 $\mu g\,m^{-3}$), a total of 10 h registered in 8 days. In addition, all days in this cluster registered at least one 8 h moving average greater than 120 $\mu g\,O_3\,m^{-3}$. The majority of the days in this cluster were categorized as non-NPF events (72.9% of the days), and only one Class II NPF event was detected (1.7% of the days). However, burst-like events occurred at a higher rate in this cluster compared to the others (see the sharp increase in concentration at 08:00 in Fig. 3). This cluster was characterized by the highest N, $N_{9-25}$, CS, solar radiation, and temperature, and the lowest relative humidity. Transported pollution made an important contribution to the cluster, as suggested by the highest wind speed (with peaks around 13:00 that point to the arrival of the BMA plume), as well as the highest BC and $SO_2$, both increasing simultaneously from 09:00 and peaking after midday with the wind speed (Table 2). N peaked at 15:00, simultaneously with BC; thus, we may interpret that the high UFP concentrations of this cluster – the highest of all clusters – were not attributable to NPF, but to the transport of highly polluted air masses from the BMA. In addition, $N_{9-25}$ exhibited two peaks (Fig. 1), the earliest one coinciding in time with the main $N_{9-25}$ peak associated with the "low" cluster and with the highest $SO_2$ peak for the "high" cluster. This suggests that during this early peak, the high $SO_2$ (and $O_3$) might have given rise to NPF, in spite of a relatively large CS.

The $O_3$ pattern in the "high" cluster occurred mostly in the summer, with a few events in April, and 218 days (25% of the period) were assigned to this cluster. Almost half the days in this cluster (104 days) registered 8 h moving averages greater than 120 $\mu g\,O_3\,m^{-3}$. These days had high solar radiation and temperature, low relative humidity, and an important contribution from transported pollutants and precursors, as suggested by the high peaks for wind speed around 13:00. High levels of BC, $SO_2$, N, and $N_{9-25}$ were registered in this cluster (Table 2). NPF occurred only in 6.9% of the days in this cluster; therefore, transported UFP emissions were accountable for the majority of the high UFP concentrations. When NPF occurred, the range of values for GRs was high within this cluster, indicating that the transported precursors also contributed to rapidly growing newly formed particles.

The $O_3$ pattern in the "mild" cluster was found mainly in the spring and late summer, and 352 days (41% of the period) were assigned to this cluster. Only 12 days in this cluster (3% of the days) register 8 h moving averages greater than 120 $\mu g\,O_3\,m^{-3}$. The cluster was mainly characterized by mild temperature, high relative humidity, and a moderate contribution of pollutants from regional transport (Table 2). NPF was relatively frequent (11.3% of the days within the cluster), although N and $N_{9-25}$ levels were relatively low. This cluster also had the highest values and range for GRs. Thus, the cluster included days with high concentrations of condensable vapors that caused high particle growth rates, as well as days when the concentration of these vapors was very low and particles grew slowly.

The $O_3$ daily pattern in the "low" cluster was found mainly in the spring and September, and this cluster consisted of 234 days (27% of the period). There were no exceedances of the hourly or 8 h $O_3$ thresholds within this cluster. NPF was detected in 12% of the days, the highest fraction of all clusters. CS, N, and $N_{9-25}$ were lower than in the other clusters. These days were characterized by the lowest solar radiation, temperature, and wind speed and the highest relative humidity (Table 2). The low concentrations of BC and $SO_2$ also suggest that pollutants were not transported to the station. According to Fig. 3, this cluster had the lowest average number particle concentrations of all diameters, but especially those larger than 100 nm. For days registering NPF, the growth rates in this cluster had the lowest range and the lowest 3rd quartile. This suggests that despite NPF being frequent during these days, there were less condensable vapors that caused particle growth, and, therefore, the particles grew more slowly than in days in other
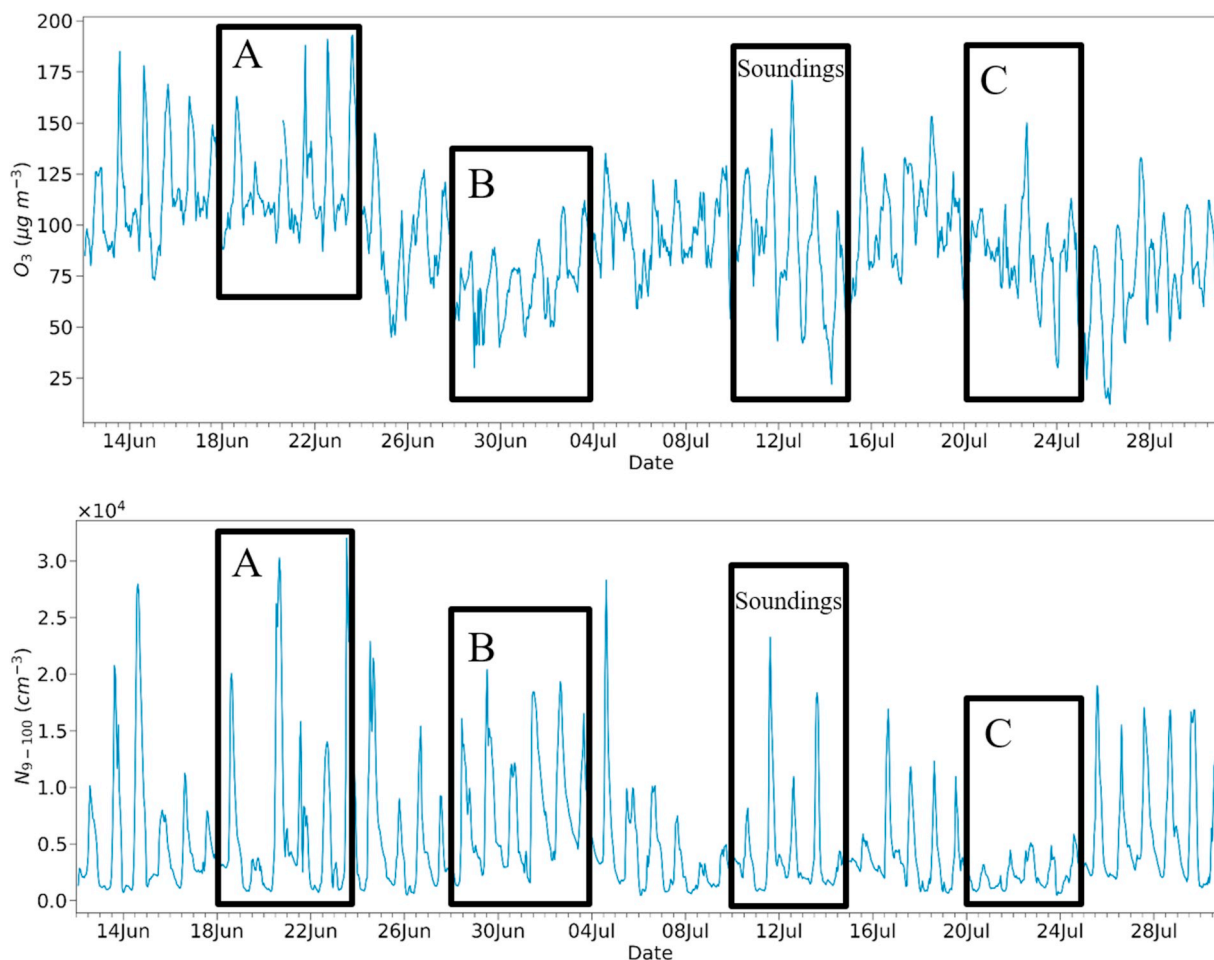
**Fig. 6.** Hourly concentrations of ozone ($O_3$) and ultrafine particles (UFPs, in the size range 9–100 nm) at Montseny during the field study between 12 June and 31 July 2017. Three cases are highlighted: A is an example of a period of extreme $O_3$ concentrations; B is an example of low $O_3$ levels; and C is an example of low UFP concentrations. The period when the balloon soundings were made is also highlighted.

clusters.

In summary, clustering based on $O_3$ concentrations revealed an apparent time correlation between $O_3$ concentrations and aerosol number concentrations, but different time patterns between high $O_3$ concentrations and NPF events with a marked impact on total N. We explore this connection in the following subsections.

### 3.2. Intensive field measurements

During the intensive field study from 12 June 2017 to 31 July 2017 at Montseny, a total of 49 days could be classified according to the cluster analysis described in section 3.1. Of these, 10 days were classified as falling within the "extreme" cluster, 17 within "high", 15 within "mild", and 7 within "low". For each cluster, the average cycles of the concentration of negative ions measured with the AIS, and the concentration of particles in the size range 1.15–2.6 nm ($N_{1.15-2.6}$) measured with the PSM are presented in Figs. 4 and 5, respectively. Fig. 6 shows the evolution of $O_3$ and UFP concentrations during the field study.

Days recording the most NPF events (days assigned to the "low" cluster) had the highest negative ion concentration, with relatively stable concentrations throughout the day with a peak at 2100 cm$^{-3}$ at 11:00 UTC. All the other clusters registered their minimum at that time (around 1000 cm$^{-3}$), while the maximums were recorded at 13:30 UTC (around 1700 cm$^{-3}$). $N_{1.15-2.6}$ was also highest for clusters registering the most NPF episodes ("low" and "mild"). However, due to technical issues, several days of PSM data were missing, and only 30 days were used to calculate the daily cycles, resulting in the high uncertainties

shown in Fig. 5.

From 10 to 14 July 2017, balloon soundings were made at the station. During this period, the middle levels of the troposphere were dominated by westerly winds, with low pressure systems located in northern Europe, and an anticyclonic ridge affecting the Southern Mediterranean, which caused stagnation of air masses over this area (see synoptic maps in Fig. S3). $O_3$ concentrations were very high, with maximum hourly values exceeding 170 µg $O_3$ m$^{-3}$. Three days, 10–12 July, were assigned to the "high" cluster, and two days, 13 and 14 July, to the "mild" cluster. No NPF events were observed in this period, although the aerosol loads were high. These observations were consistent with the cluster analysis summary presented in Table 2 for clusters "high" and "mild".

Fig. 7 shows the most representative vertical measurements obtained with the balloon soundings on 10 and 12 July. Both days were assigned to the "high" classified as cluster; therefore "high", hence, according to Table 2, it is expected to observe sea or land breezes are suggested to that transport pollutants to the station. On 10 July, $O_3$ and $N_3$ concentrations were relatively low all day and at all levels. Concentrations were constant with altitude, excluding the lowest part of the sounding, due to deposition of $O_3$ at the surface and consumption by NO. The potential temperature (θ) and water vapor mixing ratio (r) profiles corresponding to the first sounding (09:57 UTC) suggested the presence of a stable layer near the surface level (up to about 50 m) that was diluted by the sounding at 16:35 UTC. The wind speed profile was consistent with a sea or land breeze at both soundings, as expected. The morning and afternoon soundings were very similar suggesting that pollutants and
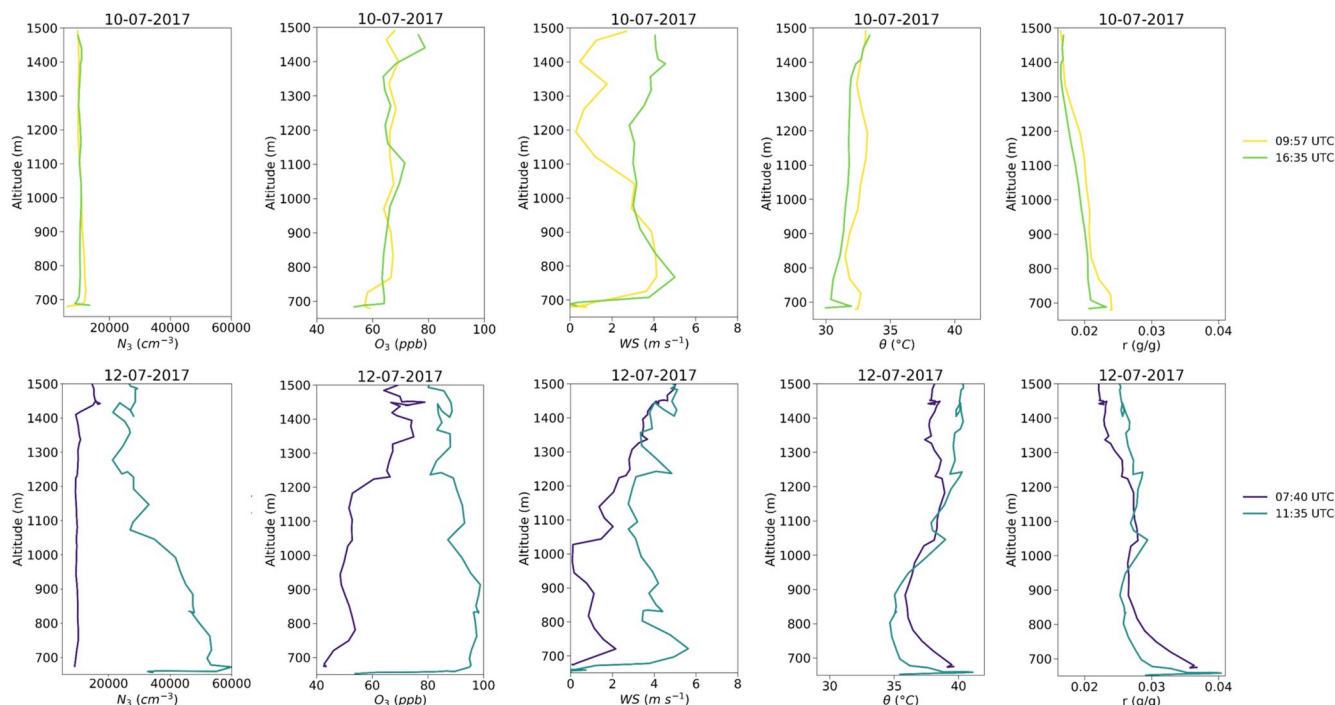
**Fig. 7.** Vertical soundings of the total number of particles with diameter >3 nm ($N_3$), ozone ($O_3$) concentration, wind speed (WS), potential temperature ($\theta$), and water vapor mixing ratio ($r$) at Montseny on 10 July 2017 (top row) and 12 July 2017 (bottom row). Note that the balloon flight times are different on the two days. The profiles at 09:57 UTC on 10 July and 07:40 UTC on 12 July correspond to ascending flights; the profiles at 16:35 UTC on 10 July and 11:35 UTC on 12 July correspond to descending flights.

precursors were not transported into the station, contrary to the results shown in Table 2.

On 12 July, $O_3$ and $N_3$ concentrations at 07:40 UTC were similar to those recorded on 10 July. At 10:40, $O_3$ and $N_3$ concentrations were notably higher, especially in a vertical extension of 200 m above ground level; maximum concentrations of 194 µg $O_3$ m$^{-3}$ and $6 \times 10^4$ particles cm$^{-3}$ were recorded. It is important to highlight that $N_3$ and $O_3$ concentrations showed a similar pattern at midday, when the mixing layer was the highest (sounding at 10:44 UTC, 12 July); concentrations were the lowest at ground level (around 650 m a.s.l.) and maximum at about 900 m a.s.l. The differences in the profiles at morning and midday and the wind speed profiles were consistent with a sea breeze that transported a polluted air mass from the Mediterranean, which had been recirculating for one or more days. This is associated with an increase in pollutant and UFP concentrations, and, therefore, high CS, which inhibited NPF. This is consistent with the summary presented in Table 2 for the "high" cluster. Similar observations were also reported by Carnerero et al. (2018) and Querol et al. (2018) during an intensive balloon soundings study in Madrid.

### 3.3. Case studies of $O_3$, UFP and NPF episodes

For an in-depth analysis of the different time patterns of $O_3$ and major NPF episodes, we selected as case studies observations for three different episodes (Cases A to C) during the field study performed at Montseny from 12 June to 31 July 2017, which are discussed in detail below. The hourly concentrations of $O_3$ and $N_{9-100}$ at Montseny throughout the study are shown in Fig. 6. The corresponding PNSD, combining AIS size spectra of negative ions in the size range 0.8–20 nm and SMPS data in the size range 20–855 nm, are shown in Fig. 8. Note that the lower half of the figure only accounts for the negative ions measured with the AIS, while the upper half represents the concentration of all charged particles (negative and positive) measured with the SMPS. Therefore, the concentrations at the boundary between the two distributions differ. Further information about these differences and a

comparison between AIS and other instruments, including a differential mobility particle sizer, are found in Gagné et al. (2011). Fig. 9 shows the averages of 30 min $N_{1.15-2.6}$ (PSM) and $N_{9-100}$ (SMPS), and Fig. 10 shows the 30 min averages of the CS. In addition, Figs. S4, S5, and S6 show the daily synoptic conditions (geopotential height at 500 hPa and mean sea level pressure at 12:00 UTC) for each case study.

Case A (18–23 June 2017) comprises a period of very high $O_3$ concentrations. A heatwave affected the area during this period, as a consequence of an anticyclonic ridge over the Iberian Peninsula and the presence of a very warm air mass transported from North Africa. Maximum temperatures over 30 °C and minimum temperatures over 20 °C were registered during the episode. Maximum $O_3$ hourly concentrations exceeded 180 µg m$^{-3}$ on three consecutive days (21–23 June), and a maximum hourly concentration of 193 µg $O_3$ m$^{-3}$ was registered, the most severe episode at Montseny since $O_3$ measurements started in 2008. All the days in this period were assigned to the "extreme" cluster, which agrees with the description for this cluster presented in Table 2.

The PNSD reveals only two weak NPF episodes on 19 and 20 June, coinciding with the lowest $O_3$ concentrations for this case (Fig. 8). The size distribution of these two events (classic "banana" events) suggests that NPF occurred over a vast area (Manninen et al., 2010). During the remaining days, fluctuations in the concentration of the finest particles detected with the AIS were observed around 06:00 UTC, although this was not necessarily related to NPF (Manninen et al., 2010). This was consistent with the concentration of particles measured with the PSM and SMPS (Fig. 9): around 06:30 UTC, the concentration of total UFPs and the CS ($6 \times 10^{-3}$ s$^{-1}$; Fig. 10) were at their minimum, while a maximum for $N_{1.15-2.6}$ concentration was registered simultaneously. This may be related to the initial stages of NPF, although growth above 10 nm was not observed. Later, the breeze transported regionally generated pollutants to the station, which was reflected by an increase in CS ($18 \times 10^{-3}$ s$^{-1}$) and $N_{9-100}$, both peaking at midday. It is plausible that the increased CS subsequently stopped the NPF process and the particles formed in the morning hours never reached sizes above 10 nm.

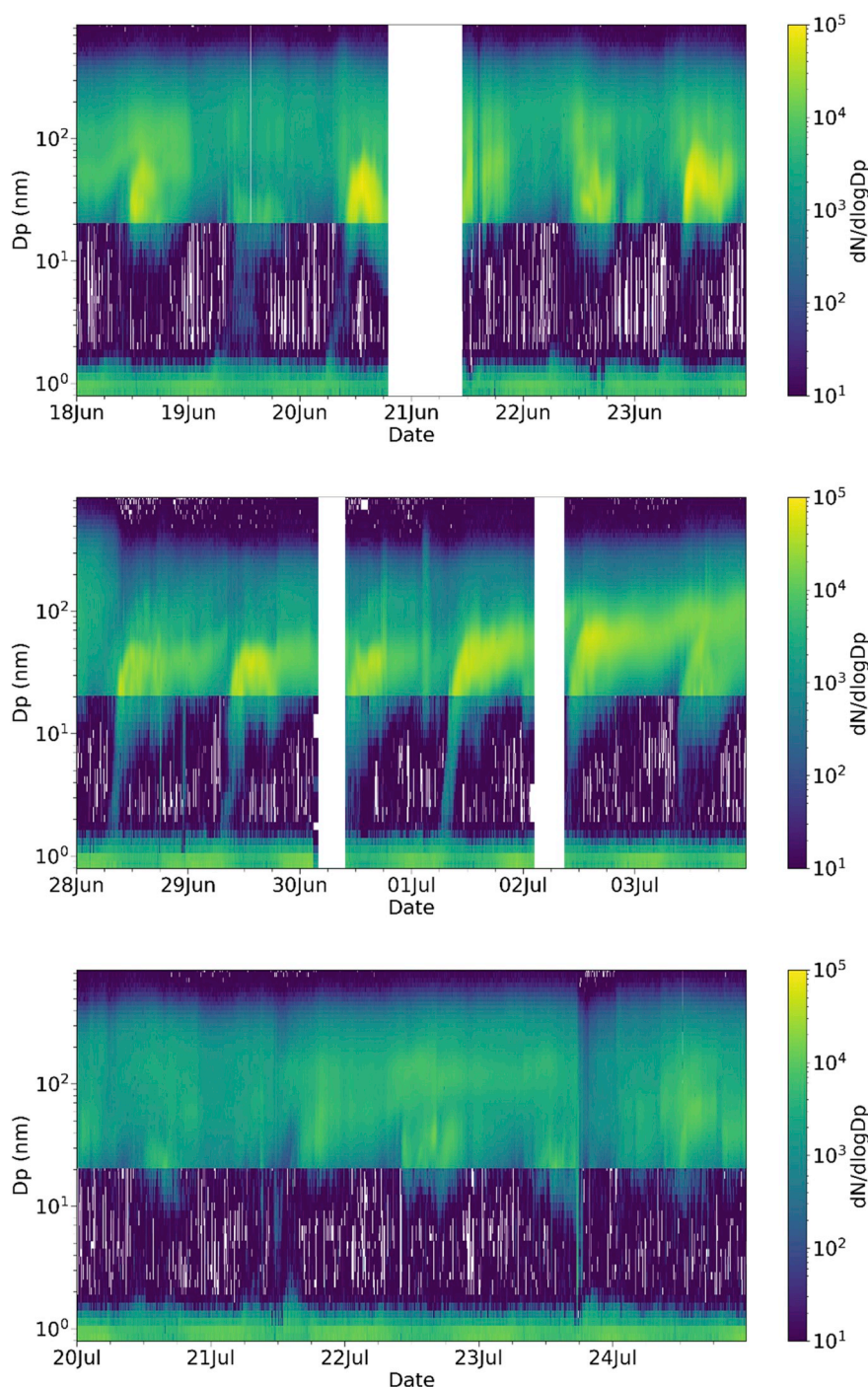Case B (28 June–3 July 2017) was a period with relatively low

**Fig. 8.** Size distribution spectra combining air ion spectrometer (negative ions, 0.8–20.0 nm) and scanning mobility particle spectrometer (20–856 nm) readings for the case studies A, B, and C (from top to bottom). Case study A is an example of a period of extreme ozone ($O_3$) concentrations, B an example of low $O_3$ levels, and C an example of low ultrafine particle concentrations. Missing data and values below the detection limit of the instruments are represented in white.

concentrations of $O_3$. The lowest temperatures (both maxima and minima) of the summer were recorded during this period. From 28 to 30 June, there were frequent and intense storms in the area as a consequence of the passage of a front and the associated entrance of a cold air mass. During this period, there were intense regional NPF Class I events starting around 11:00 UTC every day (Fig. 8), coinciding with relatively low $O_3$ concentrations (days between 28 June and 2 July were assigned to the "low" cluster; 3 July was assigned to the "mild" cluster). The low temperatures and $O_3$ concentrations agreed with the description for clusters "low" and "mild" clusters in Table 2.

Fig. 9 shows data consistent with the occurrence of the events: $N_{1.15-}$

$_{2.6}$ concentration increased until 10:30 UTC, after $N_{9-100}$ started increasing but before it peaked at midday. The influence of pollution from the BMA was limited during these days, as shown also by lower CS (ranging from $3 \times 10^{-3} \, s^{-1}$ at 07:00 UTC to $8 \times 10^{-3} \, s^{-1}$ at 15:30 UTC) and $N_{9-100}$ compared to those in Case A. Nevertheless, the area probably received a moderate concentration of NPF precursors in a relatively clean atmosphere with low CS and high levels of biogenic VOCs and $NH_3$. According to Van Damme et al. (2018), the area of study is one of the $NH_3$ hotspots worldwide. These are ideal ambient conditions for NPF episodes (Lehtipalo et al., 2018).

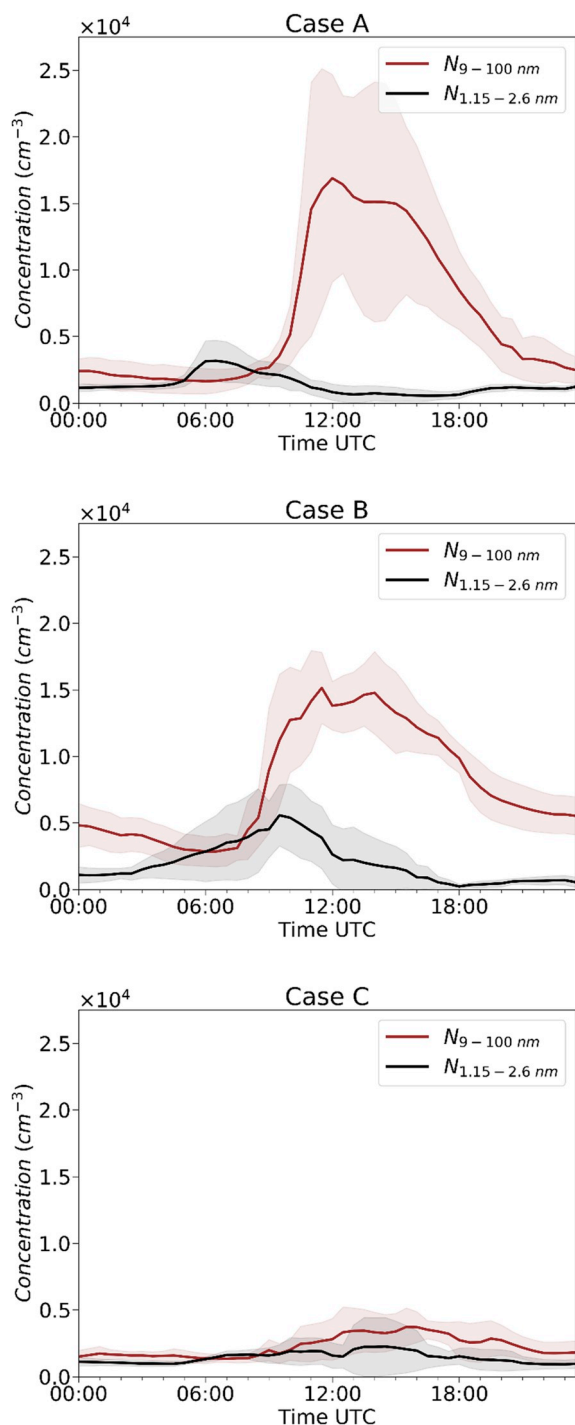Case C (20–24 July 2017) was a period with low UFPs, during which

**Fig. 9.** Thirty-minute average concentrations of particles in size ranges 1.15–2.6 nm (measured with a particle size magnifier) and 9–100 nm (measured with a scanning mobility particle spectrometer), during case study (A, B, and C) periods. Case study A is an example of a period of extreme ozone ($O_3$) concentrations, B an example of low $O_3$ levels, and C an example of low ultrafine particle concentrations. Shaded areas represent 95% confidence intervals.

the combination of an anticyclonic ridge in the Mediterranean and a low-pressure system in the North Sea caused the passage of a trough over the Iberian Peninsula, with cold air in its center. At the surface, a stationary high-pressure system caused the stagnation of warm air in the area of study. The warm air at the surface in combination with the cold air aloft favored strong thunderstorms, especially in the afternoons.
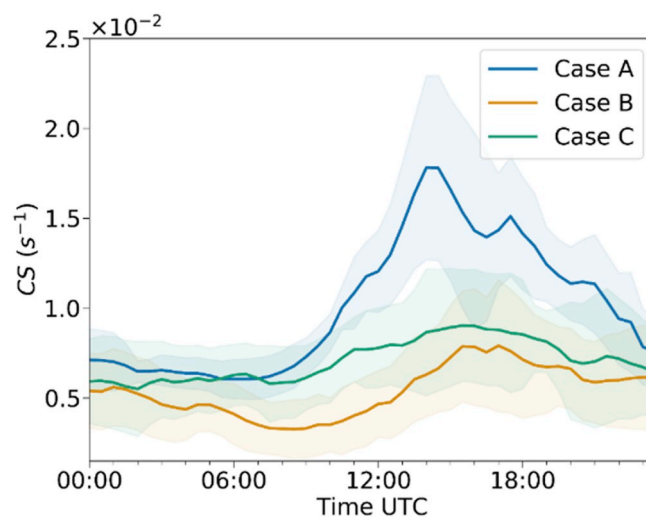


**Fig. 10.** Thirty-minute averages of the condensation sink (CS) at Montseny for cases A, B and C. Case study A is an example of a period of extreme ozone ($O_3$) concentrations, B an example of low $O_3$ levels, and C an example of low ultrafine particle concentrations. Shaded areas represent 95% confidence intervals.

During this period, UFP concentrations were very low, suggesting a low pollution load, but no NPF events were observed. This agreed with the average evolution of CS, which was higher than in Case B, when NPF was observed every day. $O_3$ concentrations were moderate, but the daily formation was low, i.e., there was no large difference in the concentrations throughout the day. In addition, the background concentration decreased during this period. For this reason, the days in this case were not assigned to a single cluster, but to "high" (22 July), "mild" (20, 21, and 24 July), and "low" (23 July) clusters. In this case, the conditions for inhibiting $O_3$ formation also inhibited NPF.

## 4. Conclusions

We studied the simultaneity of the occurrence of peak episodes of $O_3$, UFPs, and NPF in a regional background station located 40 km often downwind of the BMA in northeast Spain in the Western Mediterranean, between April and September in 2014–2018. In addition, the concentrations of negative ions and particles <3 nm were measured during a field study from 12 June to 31 July 2017. The vertical distribution of pollutants up to 1500 m above ground level was determined from 10 to 14 July 2017.

During these warm periods, the results indicate that the highest UFP concentrations coincided with the highest $O_3$ episodes. However, the probability of NPF with particles growing to >25 nm (according to the definition of an NPF episode) was the lowest during these days, even though the nucleation-mode number concentration was the highest due to the contribution of traffic emissions and growth rates were high due to high concentrations of condensable vapors. In this period, temperature, solar radiation, and wind speed were at their highest, and relative humidity at its lowest. The CS and concentrations of BC and $SO_2$ were also at a maximum. This suggests that pollutants are recirculated and/or transported from the BMA and other populated and industrial areas to the station during warm periods. Conversely, when the transported air mass is relatively clean and there is no recirculation, especially during and after the passage of weather fronts, UFP and $O_3$ concentrations are at their lowest, and NPF is most favored, although growth rates are at their lowest. This may be because high $O_3$ episodes at Montseny require polluted air masses (with high levels of particles, and accordingly CS) being transported from the valleys and the BMA. On the other hand, NPF requires either high precursor concentrations or clean atmospheres when precursor concentrations are low. However, when the atmosphere

is too clean, for example during the passage of a cold front causing strong convection and instability, the concentrations of NPF precursors are too low, and loss rates are greater than formation rates, thus the formation of particles is not detected. In addition, the concentration of newly formed particles in this case is low compared to the background particle number concentration. Thus, it is important to be aware of the scales of background and episode concentrations at the location of study. For example, NPF has been described in the Artic with much lower concentrations of precursors (Nieminen et al., 2018).

In essence, summertime vertical recirculation of Wester Mediterranean air masses is a major cause of regional $O_3$ pollution episodes, and it is also responsible for enrichment of aerosol particles and particle precursors, which results in high levels of UFPs associated with higher $O_3$. This increases the CS to the point that NPF is inhibited. On the other hand, in the absence of recirculation and during its initial stages, humid air masses with NPF precursors are transported inland by the diurnal local-scale circulations (Millán et al., 1997). These are diluted into dryer and warmer rural air masses, enriched with biogenic volatile organic compounds and $NH_3$. This is the optimum scenario for NPF in air masses with relatively low $O_3$ background concentrations (Lehtipalo et al., 2018). However, the dynamics of $O_3$, UFP, and NPF episodes are very complex, and we cannot conclude that these episodes are either simultaneous or mutually excluding. Further studies are needed to better understand these intense episodes.

With regard to implications for air quality, the occurrence of the highest $O_3$ episodes with the highest UFP levels may magnify the health impacts of the episodes. The transported UFPs consist of both primary and secondary particles. During the lowest (but still high in absolute concentration) spring–summer $O_3$ episodes (days in the "low" cluster), the contribution of primary UFPs is very low, with UFPs being mainly secondary resulting from NPF. The health impact of UFPs in these two distinct types of episodes is probably different, as reported by Tobías et al. (2018) when evaluating the health outcomes of traffic-related and bulk UFP concentrations in Barcelona. They reported that NPF-dominated days were associated with low premature mortality risk, because these episodes were linked with less polluted days. During these days, the total number of particles is the lowest, as we have demonstrated in this study.

### Declaration of competing interest

The authors declare that they have no known competing financial interests or personal relationships that could have appeared to influence the work reported in this paper.

### Acknowledgments

### Appendix A. Supplementary data

Supplementary data to this article can be found online at https://doi.org/10.1016/j.aeaoa.2019.100051.

## References

Atkinson, R.W., Fuller, G.W., Anderson, H.R., Harrison, R.M., Armstrong, B., 2010. Urban ambient particle metrics and health. Epidemiology 21 (4), 501–511. https://doi.org/10.1097/EDE.0b013e3181debc88.

Boy, M., Kulmala, M., 2002. Nucleation events in the continental boundary layer: influence of physical and meteorological parameters. Atmos. Chem. Phys. https://doi.org/10.5194/acp-2-1-2002.

Brines, M., Dall'Osto, M., Beddows, D.C.S., Harrison, R.M., Gómez-Moreno, F., Núñez, L., Artíñano, B., Costabile, F., Gobbi, G.P., Salimi, F., Morawska, L., Sioutas, C., Querol, X., 2015. Traffic and nucleation events as main sources of ultrafine particles in high-insolation developed world cities. Atmos. Chem. Phys. https://doi.org/10.5194/acp-15-5929-2015.

Carnerero, C., Pérez, N., Reche, C., Ealo, M., Titos, G., Lee, H.-K., Eun, H.-R., Park, Y.-H., Dada, L., Paasonen, P., Kerminen, V.-M., Mantilla, E., Escudero, M., Gómez-Moreno, F.J., Alonso-Blanco, E., Coz, E., Saiz-Lopez, A., Temime-Roussel, B., Marchand, N., Beddows, D.C.S., Harrison, R.M., Petäjä, T., Kulmala, M., Ahn, K.-H., Alastuey, A., Querol, X., 2018. Vertical and horizontal distribution of regional new particle formation events in Madrid. Atmos. Chem. Phys. 18 (22), 16601–16618. https://doi.org/10.5194/acp-18-16601-2018.

Chu, B., Kerminen, V.-M., Bianchi, F., Yan, C., Petäjä, T., Kulmala, M., 2019. Atmospheric new particle formation in China. Atmos. Chem. Phys. 19, 115–138. https://doi.org/10.5194/acp-19-115-2019.

Dal Maso, M., Kulmala, M., Riipinen, I., Wagner, R., Hussein, T., Aalto, P.P., Lehtinen, K.E.J., Maso, D., Kulmala, M., Riipinen, M., Wagner, I., Hussein, R., Aalto, T., Lehtinen, P.P., 2005. Formation and growth of fresh atmospheric aerosols: eight years of aerosol size distribution data from SMEAR II, Hyytiälä, Finland. Boreal Environ. Res. 10, 323–336.

Dall'Osto, M., Beddows, D.C.S., Pey, J., Rodriguez, S., Alastuey, A., Harrison, R.M., Querol, X., 2012. Urban aerosol size distributions over the Mediterranean city of Barcelona, NE Spain. Atmos. Chem. Phys. 12 (22), 10693–10707. https://doi.org/10.5194/acp-12-10693-2012.

Dall'Osto, M., Querol, X., Alastuey, A., O&apos, Dowd, C., Harrison, R.M., Wenger, J., Gómez-Moreno, F.J., 2013. On the spatial distribution and evolution of ultrafine particles in Barcelona. Atmos. Chem. Phys. 13 (2), 741–759. https://doi.org/10.5194/acp-13-741-2013.

Van Damme, M., Clarisse, L., Whitburn, S., Hadji-Lazaro, J., Hurtmans, D., Clerbaux, C., Coheur, P.-F., 2018. Industrial and agricultural ammonia point sources exposed. Nature 564 (7734), 99–103. https://doi.org/10.1038/s41586-018-0747-1.

EC Directive 2008/50/EC of 21 May 2008, 2008. On ambient air quality and cleaner air for Europe [online] Available from: https://eur-lex.europa.eu/legal-content/EN/TXT/HTML/?uri=CELEX:32008L0050&from=ES. (Accessed 31 January 2019).

EEA, 2018. Air Quality in Europe — 2018 Report.

Fernández-Camacho, R., Rodríguez, S., De La Rosa, J., Sánchez De La Campa, A.M., Viana, M., Alastuey, A., Querol, X., 2010. Ultrafine particle formation in the inland sea breeze airflow in Southwest Europe. Atmos. Chem. Phys. 10, 9615–9630. https://doi.org/10.5194/acp-10-9615-2010.

Gagné, S., Lehtipalo, K., Manninen, H.E., Nieminen, T., Schobesberger, S., Franchin, A., Yli-Juuti, T., Boulon, J., Sonntag, A., Mirme, S., Mirme, A., Hõrrak, U., Petäjä, T., Asmi, E., Kulmala, M., 2011. Atmospheric Measurement Techniques Intercomparison of air ion spectrometers: an evaluation of results in varying conditions. Atmos. Meas. Tech. 4, 805–822. https://doi.org/10.5194/amt-4-805-2011.

Gonçalves, M., Jiménez-Guerrero, P., Baldasano, J.M., 2009. Contribution of atmospheric processes affecting the dynamics of air pollution in South-Western Europe during a typical summertime photochemical episode. Atmos. Chem. Phys. 9 (3), 849–864. https://doi.org/10.5194/acp-9-849-2009.

Gordon, H., Kirkby, J., Baltensperger, U., Bianchi, F., Breitenlechner, M., Curtius, J., Dias, A., Dommen, J., Donahue, N.M., Dunne, E.M., Duplissy, J., Ehrhart, S., Flagan, R.C., Frege, C., Fuchs, C., Hansel, A., Hoyle, C.R., Kulmala, M., Kürten, A., Lehtipalo, K., Makhmutov, V., Molteni, U., Rissanen, M.P., Stozkhov, Y., Tröstl, J., Tsagkogeorgas, G., Wagner, R., Williamson, C., Wimmer, D., Winkler, P.M., Yan, C., Carslaw, K.S., 2017. Causes and importance of new particle formation in the present-day and preindustrial atmospheres. J. Geophys. Res. Atmos. 122 (16), 8739–8760. https://doi.org/10.1002/2017JD026844.

Hussein, T., Dal Maso, M., Petaja, T., Koponen, I.K., Paatero, P., Aalto, P.P., Hameri, K., Kulmala, M., 2005. Evaluation of an automatic algorithm for fitting the particle number size distributions. Boreal Environ. Res. 10 (5), 337–355.

Kalabokas, P., Hjorth, J., Foret, G., Dufour, G., Eremenko, M., Siour, G., Cuesta, J., Beekmann, M., 2017. An investigation on the origin of regional springtime ozone episodes in the Western Mediterranean. Atmos. Chem. Phys. 17 (6), 3905–3928. https://doi.org/10.5194/acp-17-3905-2017.

Kalabokas, P.D., Volz-Thomas, A., Brioude, J., Thouret, V., Cammas, J.-P., Repapis, C.C., 2007. Vertical ozone measurements in the troposphere over the Eastern Mediterranean and comparison with central Europe. Atmos. Chem. Phys. 7 (14), 3783–3790. https://doi.org/10.5194/acp-7-3783-2007.

Kangasluoma, J., Attoui, M., Junninen, H., Lehtipalo, K., Samodurov, A., Korhonen, F., Sarnela, N., Schmidt-Ott, A., Worsnop, D., Kulmala, M., Petäjä, T., 2015. Sizing of neutral sub 3 nm tungsten oxide clusters using airmodus particle size magnifier. J. Aerosol Sci. 87, 53–62. https://doi.org/10.1016/J.JAEROSCI.2015.05.007.

Kangasluoma, J., Franchin, A., Duplissy, J., Ahonen, L., Korhonen, F., Attoui, M., Mikkilä, J., Lehtipalo, K., Vanhanen, J., Kulmala, M., Petäjä, T., 2016. Operation of the Airmodus A11 nano Condensation Nucleus Counter at various inlet pressures and various operation temperatures, and design of a new inlet system. Atmos. Meas. Tech. 9, 2977–2988. https://doi.org/10.5194/amt-9-2977-2016.

Kecorius, S., Kivekäs, N., Kristensson, A., Tuch, T., Covert, D.S., Birmili, W., Lihavainen, H., Hyvärinen, A.-P., Martinsson, J., Sporre, M.K., Swietlicki, E., Wiedensohler, A., Ulevicius, V., 2016. Significant increase of aerosol number concentrations in air masses crossing a densely trafficked sea area. Oceanologia 58 (1), 1–12. https://doi.org/10.1016/J.OCEANO.2015.08.001.

Kerminen, V.-M., Chen, X., Vakkari, V., Petäjä, T., Kulmala, M., Bianchi, F., 2018. Atmospheric new particle formation and growth: review of field observations. Environ. Res. Lett. 13 (10), 103003. https://doi.org/10.1088/1748-9326/aadf3c.

Keuken, M.P., Moerman, M., Zandveld, P., Henzing, J.S., Hoek, G., 2015. Total and size-resolved particle number and black carbon concentrations in urban areas near Schiphol airport (The Netherlands). Atmos. Environ. 104, 132–142. https://doi.org/10.1016/J.ATMOSENV.2015.01.015.

Keuken, M.P., Moerman, M., Zandveld, P., Henzing, J.S., 2015. Total and size-resolved particle number and black carbon concentrations near an industrial area. Atmos. Environ. 122, 196–205. https://doi.org/10.1016/J.ATMOSENV.2015.09.047.

Kulmala, M., Petäjä, T., Nieminen, T., Sipilä, M., Manninen, H.E., Lehtipalo, K., Dal Maso, M., Aalto, P.P., Junninen, H., Paasonen, P., Riipinen, I., Lehtinen, K.E.J., Laaksonen, A., Kerminen, V.-M., 2012. Measurement of the nucleation of atmospheric aerosol particles. Nat. Protoc. 7 (9), 1651–1667. https://doi.org/10.1038/nprot.2012.091.

Kumar, P., Morawska, L., Birmili, W., Paasonen, P., Hu, M., Kulmala, M., Harrison, R.M., Norford, L., Britter, R., 2014. Ultrafine particles in cities. Environ. Int. 66, 1–10. https://doi.org/10.1016/J.ENVINT.2014.01.013.

Lanzinger, S., Schneider, A., Breitner, S., Stafoggia, M., Erzen, I., Dostal, M., Pastorkova, A., Bastian, S., Cyrys, J., Zscheppang, A., Kolodnitska, T., Peters, A., 2016. Associations between ultrafine and fine particles and mortality in five central European cities — results from the UFIREG study. Environ. Int. 88, 44–52. https://doi.org/10.1016/J.ENVINT.2015.12.006.

Lee, H.-K., Hwang, I.-K., Ahn, K.-H., 2014. Development and evaluation of Hy-CPC, part. Aerosol Res. 10 (93–97).

Lehtipalo, K., Yan, C., Dada, L., Bianchi, F., Xiao, M., Wagner, R., Stolzenburg, D., Ahonen, L.R., Amorim, A., Baccarini, A., Bauer, P.S., Baumgartner, B., Bergen, A., Bernhammer, A.-K., Breitenlechner, M., Brilke, S., Buchholz, A., Mazon, S.B., Chen, D., Chen, X., Dias, A., Dommen, J., Draper, D.C., Duplissy, J., Ehn, M., Finkenzeller, H., Fischer, L., Frege, C., Fuchs, C., Garmash, O., Gordon, H., Hakala, J., He, X., Heikkinen, L., Heinritzi, M., Helm, J.C., Hofbauer, V., Hoyle, C.R., Jokinen, T., Kangasluoma, J., Kerminen, V.-M., Kim, C., Kirkby, J., Kontkanen, J., Kürten, A., Lawler, M.J., Mai, H., Mathot, S., Mauldin, R.L., Molteni, U., Nichman, L., Nie, W., Nieminen, T., Ojdanic, A., Onnela, A., Passananti, M., Petäjä, T., Piel, F., Pospisilova, V., Quéléver, L.L.J., Rissanen, M.P., Rose, C., Sarnela, N., Schallhart, S., Schuchmann, S., Sengupta, K., Simon, M., Sipilä, M., Tauber, C., Tomé, A., Tröstl, J., Väisänen, O., Vogel, A.L., Volkamer, R., Wagner, A.C., Wang, M., Weitz, L., Wimmer, D., Ye, P., Ylisirniö, A., Zha, Q., Carslaw, K.S., Curtius, J., Donahue, N.M., Flagan, R.C., Hansel, A., Riipinen, I., Virtanen, A., Winkler, P.M., Baltensperger, U., Kulmala, M., Worsnop, D.R., 2018. Multicomponent new particle formation from sulfuric acid, ammonia, and biogenic vapors. Sci. Adv. 4 (12), eaau5363. https://doi.org/10.1126/sciadv.aau5363.

Ma, N., Birmili, W., 2015. Estimating the contribution of photochemical particle formation to ultrafine particle number averages in an urban atmosphere. Sci. Total Environ. 512–513, 154–166. https://doi.org/10.1016/J.SCITOTENV.2015.01.009.

Manninen, H.E., Nieminen, T., Asmi, E., Gagné, S., Häkkinen, S., Lehtipalo, K., Aalto, P., Vana, M., Mirme, A., Mirme, S., Hõrrak, U., Plass-Dülmer, C., Stange, G., Kiss, G., Hoffer, A., Törő, N., Moerman, M., Henzing, B., de Leeuw, G., Brinkenberg, M., Kouvarakis, G.N., Bougiatioti, A., Mihalopoulos, N., O'Dowd, C., Ceburnis, D., Arneth, A., Svenningsson, B., Swietlicki, E., Tarozzi, L., Decesari, S., Facchini, M.C., Birmili, W., Sonntag, A., Wiedensohler, A., Boulon, J., Sellegri, K., Laj, P., Gysel, M., Bukowiecki, N., Weingartner, E., Wehrle, G., Laaksonen, A., Hamed, A., Joutsensaari, J., Petäjä, T., Kerminen, V.-M., Kulmala, M., 2010. EUCAARI ion spectrometer measurements at 12 European sites – analysis of new particle formation events. Atmos. Chem. Phys. 10 (16), 7907–7927. https://doi.org/10.5194/acp-10-7907-2010.

Millán, M.M., Artíñano, B., Alonso, L., Navazo, M., Castro, M., 1991. The effect of meso-scale flows on regional and long-range atmospheric transport in the Western Mediterranean area. Atmos. Environ. Part A. Gen. Top. 25 (5–6), 949–963. https://doi.org/10.1016/0960-1686(91)90137-V.

Millán, M.M., Salvador, R., Mantilla, E., Kallos, G., 1997. Photooxidant dynamics in the Mediterranean basin in summer: results from European research projects. J. Geophys. Res. Atmos. 102 (D7), 8811–8823. https://doi.org/10.1029/96JD03610.

Millán, M.M., Mantilla, E., Salvador, R., Carratalá, A., Sanz, M.J., Alonso, L., Gangoiti, G., Navazo, M., Millán, M.M., Mantilla, E., Salvador, R., Carratalá, A., Sanz, M.J., Alonso, L., Gangoiti, G., Navazo, M., 2000. Ozone cycles in the Western Mediterranean basin: interpretation of monitoring data in complex coastal terrain. J. Appl. Meteorol. 39 (4), 487–508. https://doi.org/10.1175/1520-0450(2000)039<0487:OCITWM>2.0.CO;2.

Minoura, H., Takekawa, H., 2005. Observation of number concentrations of atmospheric aerosols and analysis of nanoparticle behavior at an urban background area in Japan. Atmos. Environ. 39 (32), 5806–5816. https://doi.org/10.1016/J.ATMOSENV.2005.06.033.

Mirme, A., Tamm, E., Mordas, G., Vana, M., Uin, J., Mirme, S., Bernotas, T., Laakso, L., Hirsikko, A., Kulmala, M., 2007. A wide-range multi-channel air ion spectrometer. Boreal Environ. Res. 12 (3), 247–264 [online] Available from: https://pdfs.semanticscholar.org/01fa/9a8eb45aafee02a4d4c20d3230a7fa7554e0.pdf. (Accessed 11 April 2019).

Monks, P.S., Archibald, A.T., Colette, A., Cooper, O., Coyle, M., Derwent, R., Fowler, D., Granier, C., Law, K.S., Mills, G.E., Stevenson, D.S., Tarasova, O., Thouret, V., Von Schneidemesser, E., Sommariva, R., Wild, O., Williams, M.L., 2015. Tropospheric ozone and its precursors from the urban to the global scale from air quality to short-lived climate forcer. Atmos. Chem. Phys. https://doi.org/10.5194/acp-15-8889-2015.

Németh, Z., Rosati, B., Zíková, N., Salma, I., Bozó, L., Dameto de España, C., Schwarz, J., Ždímal, V., Wonaschütz, A., 2018. Comparison of atmospheric new particle formation events in three Central European cities. Atmos. Environ. 178, 191–197. https://doi.org/10.1016/J.ATMOSENV.2018.01.035.

Nieminen, T., Kerminen, V.-M., Petäjä, T., Aalto, P.P., Arshinov, M., Asmi, E., Baltensperger, U., Beddows, D.C.S., Beukes, J.P., Collins, D., Ding, A., Harrison, R. M., Henzing, B., Hooda, R., Hu, M., Hõrrak, U., Kivekäs, N., Komsaare, K., Krejci, R., Kristensson, A., Laakso, L., Laaksonen, A., Leaitch, W.R., Lihavainen, H., Mihalopoulos, N., Németh, Z., Nie, W., O'dowd, C., Salma, I., Sellegri, K., Svenningsson, B., Swietlicki, E., Tunved, P., Ulevicius, V., Vakkari, V., Vana, M., Wiedensohler, A., Wu, Z., Virtanen, A., Kulmala, M., 2018. Global analysis of continental boundary layer new particle formation based on long-term measurements. Atmos. Chem. Phys. 18, 14737–14756. https://doi.org/10.5194/acp-18-14737-2018.

Paasonen, P., Kupiainen, K., Klimont, Z., Visschedijk, A., Denier van der Gon, H.A.C., Amann, M., 2016. Continental anthropogenic primary particle number emissions. Atmos. Chem. Phys. 16 (11), 6823–6840. https://doi.org/10.5194/acp-16-6823-2016.

Park, K., Park, J.Y., Kwak, J.-H., Cho, G.N., Kim, J.-S., 2008. Seasonal and diurnal variations of ultrafine particle concentration in urban Gwangju, Korea: observation of ultrafine particle events. Atmos. Environ. 42 (4), 788–799. https://doi.org/10.1016/J.ATMOSENV.2007.09.068.

Pedregosa, F., Varoquaux, A., Gramfort, A., Michel, V., Thirion, B., Grisel, O., Blondel, M., Prettenhofer, P., Weiss, R., Dubourg, V., Vanderplas, J., Passos, A., Cournapeau, D., Brucher, M., Perrot, M., Duchesnay, É., 2011. Scikit-learn: machine learning in Python. Oct J. Mach. Learn. Res. 12, 2825–2830 [online] Available from: http://jmlr.csail.mit.edu/papers/v12/pedregosa11a.html.

Pérez, N., Pey, J., Castillo, S., Viana, M., Alastuey, A., Querol, X., 2008. Interpretation of the variability of levels of regional background aerosols in the Western Mediterranean. Sci. Total Environ. 407 (1), 527–540. https://doi.org/10.1016/J.SCITOTENV.2008.09.006.

Pey, J., Querol, X., Alastuey, A., Rodríguez, S., Putaud, J.P., Van Dingenen, R., 2009. Source apportionment of urban fine and ultra-fine particle number concentration in a Western Mediterranean city. Atmos. Environ. Times 43 (29), 4407–4415. https://doi.org/10.1016/J.ATMOSENV.2009.05.024.

Pikridas, M., Riipinen, I., Hildebrandt, L., Kostenidou, E., Manninen, H., Mihalopoulos, N., Kalivitis, N., Burkhart, J.F., Stohl, A., Kulmala, M., Pandis, S.N., 2012. New particle formation at a remote site in the Eastern Mediterranean. J. Geophys. Res. Atmos. 117 (D12) https://doi.org/10.1029/2012JD017570 n/a-n/a.

Pöschl, U., 2005. Atmospheric aerosols: composition, transformation, climate and health effects. Angew. Chem. Int. Ed. 44 (46), 7520–7540. https://doi.org/10.1002/anie.200501122.

Querol, X., Gangoiti, G., Mantilla, E., Alastuey, A., Minguillón, M.C., Amato, F., Reche, C., Viana, M., Moreno, T., Karanasiou, A., Rivas, I., Pérez, N., Ripoll, A., Brines, M., Ealo, M., Pandolfi, M., Lee, H.-K., Eun, H.-R., Park, Y.-H., Escudero, M., Beddows, D., Harrison, R.M., Bertrand, A., Marchand, N., Lyasota, A., Codina, B., Olid, M., Udina, M., Jiménez-Esteve, B., Soler, M.R., Alonso, L., Millán, M., Ahn, K.-H., 2017. Phenomenology of high-ozone episodes in NE Spain. Atmos. Chem. Phys. 17 (4), 2817–2838. https://doi.org/10.5194/acp-17-2817-2017.

Querol, X., Alastuey, A., Gangoiti, G., Perez, N., Lee, H.K., Eun, H.R., Park, Y., Mantilla, E., Escudero, M., Titos, G., Alonso, L., Temime-Roussel, B., Marchand, N., Moreta, J.R., Revuelta, M.A., Salvador, P., Artíñano, B., García dos Santos, S., Anguas, M., Notario, A., Saiz-Lopez, A., Harrison, R.M., Millán, M., Ahn, K.-H., 2018. Phenomenology of summer ozone episodes over the Madrid metropolitan area, central Spain. Atmos. Chem. Phys. 18 (9), 6511–6533. https://doi.org/10.5194/acp-18-6511-2018.

Rodríguez, S., Querol, X., Alastuey, A., Viana, M.-M., Mantilla, E., 2003. Events Affecting Levels and Seasonal Evolution of Airborne Particulate Matter Concentrations in the Western Mediterranean. https://doi.org/10.1021/ES020106P.

Salma, I., Borsós, T., Németh, Z., Weidinger, T., Aalto, P., Kulmala, M., 2014. Comparative study of ultrafine atmospheric aerosol within a city. Atmos. Environ. 92, 154–161. https://doi.org/10.1016/J.ATMOSENV.2014.04.020.

Salma, I., Németh, Z., Kerminen, V.-M., Aalto, P., Nieminen, T., Weidinger, T., Molnár, Á., Imre, K., Kulmala, M., 2016. Regional effect on urban atmospheric nucleation. Atmos. Chem. Phys. 16 (14), 8715–8728. https://doi.org/10.5194/acp-16-8715-2016.

Seco, R., Peñuelas, J., Filella, I., Llusià, J., Molowny-Horas, R., Schallhart, S., Metzger, A., Müller, M., Hansel, A., 2011. Contrasting winter and summer VOC mixing ratios at a forest site in the Western Mediterranean basin: the effect of local biogenic emissions. Atmos. Chem. Phys. 11 (24), 13161–13179. https://doi.org/10.5194/acp-11-13161-2011.

Stafoggia, M., Schneider, A., Cyrys, J., Samoli, E., Andersen, Z.J., Bedada, G.B., Bellander, T., Cattani, G., Eleftheriadis, K., Faustini, A., Hoffmann, B., Jacquemin, B., Katsouyanni, K., Massling, A., Pekkanen, J., Perez, N., Peters, A., Quass, U., Yli-Tuomi, T., Forastiere, F., 2017. Association between short-term exposure to ultrafine particles and mortality in eight European urban areas. Epidemiology 28 (2), 172–180. https://doi.org/10.1097/EDE.0000000000000599.

Tobías, A., Rivas, I., Reche, C., Alastuey, A., Rodríguez, S., Fernández-Camacho, R., Sánchez de la Campa, A.M., de la Rosa, J., Sunyer, J., Querol, X., 2018. Short-term effects of ultrafine particles on daily mortality by primary vehicle exhaust versus

secondary origin in three Spanish cities. Environ. Int. 111, 144–151. https://doi.org/10.1016/J.ENVINT.2017.11.015.

Toll, I., Baldasano, J.M., 2000. Modeling of photochemical air pollution in the Barcelona area with highly disaggregated anthropogenic and biogenic emissions. Atmos. Environ. 34 (19), 3069–3084. https://doi.org/10.1016/S1352-2310(99)00498-7.

Valverde, V., Pay, M.T., Baldasano, J.M., 2016. Ozone attributed to Madrid and Barcelona on-road transport emissions: characterization of plume dynamics over the iberian Peninsula. Sci. Total Environ. 543, 670–682. https://doi.org/10.1016/J.SCITOTENV.2015.11.070.

Vanhanen, J., Mikkilä, J., Lehtipalo, K., Sipilä, M., Manninen, H.E., Siivola, E., Petäjä, T., Kulmala, M., 2011. Particle size magnifier for nano-CN detection. Aerosol Sci. Technol. 45 (4), 533–542. https://doi.org/10.1080/02786826.2010.547889.

Wang, D., Zhou, B., Fu, Q., Zhao, Q., Zhang, Q., Chen, J., Yang, X., Duan, Y., Li, J., 2016. Intense secondary aerosol formation due to strong atmospheric photochemical reactions in summer: observations at a rural site in eastern Yangtze River Delta of China. Sci. Total Environ. 571, 1454–1466. https://doi.org/10.1016/J.SCITOTENV.2016.06.212.

WHO, 2006. WHO Air Quality Guidelines for Particulate Matter, Ozone, Nitrogen Dioxide and Sulfur Dioxide.

Wonaschütz, A., Demattio, A., Wagner, R., Burkart, J., Zíková, N., Vodička, P., Ludwig, W., Steiner, G., Schwarz, J., Hitzenberger, R., 2015. Seasonality of new particle formation in Vienna, Austria – influence of air mass origin and aerosol chemical composition. Atmos. Environ. 118, 118–126. https://doi.org/10.1016/J.ATMOSENV.2015.07.035.